Marine Structures 59 (2018) 158–178

Contents lists available at ScienceDirect

Marine Structures

journal homepage: www.elsevier.com/locate/marstruc

A macro-element for integrated time domain analyses representing bucket foundations for offshore wind turbines

K.S. Skau[a,b,*], G. Grimstad[b], A.M. Page[a,b], G.R. Eiksund[b], H.P. Jostad[a,b]

[a] Norwegian Geotechnical Institute, NGI, P.O. Box. 3930, Ullevål Stadion, N-0806 Oslo, Norway
[b] Norwegian University of Science and Technology, NO-7491 Trondheim, Norway

A B S T R A C T

The paper presents a macro-element model for bucket foundations to be used in integrated time domain analyses of offshore wind turbines. The macro-element has been formulated in the multi-surface plasticity framework, and captures the characteristic behaviour of a shallow foundation subjected to irregular cyclic loading. A numerical study of shallow foundations in clay has been used as basis for the development. In conjunction with offshore wind support structures, bucket foundations can be used as monopod foundations and in multi-leg configurations. This makes almost any combination of vertical, horizontal and moment loads relevant. The macro-element has been developed with the intention of creating an application oriented engineering model with physical interpretable input data. Three examples are used to illustrate the macro-element's performance. These examples show that the macro-element 1) reproduces the response computed in finite element analyses of the soil volume and the bucket foundation, 2) is numerically stable and does not cause numerical ratchetting, 3) produces response in good agreement with a large scale field test.

1. Introduction

Offshore wind turbines (OWTs) are dynamically sensitive structures when exposed to loads from wind, waves and current. Numerous studies have demonstrated the influence of foundation flexibility on natural frequency and structural fatigue damage of OWTs [1–4]. Published studies of field measurements of monopiles suggest that design tools generally underestimate the foundation stiffness [5,6]. Hence, efficient and accurate foundation models can improve the overall accuracy in design of OWTs. Advanced dynamic time domain analyses have become the industry standard in design. However, the foundation models used in design are often overly simplified. This paper presents a macro-element model for bucket foundations supporting OWTs.

The bucket foundation concept, used in the oil and gas industry for many years [7,8], was proposed as a foundation method for offshore wind turbines in the early 2000s [9–11]. Bucket foundations are shallow foundations with steel skirts penetrated into the soil and a closed top plate (lid). Suction caissons and suction buckets are other terms frequently used, referring to the installation method where under-pressure ("suction") is used to penetrate the skirts into the soil. The installation method has its advantage of being relatively fast and silent. However, installation in layered soil has been questioned, and this may be the main reason for the limited usage within offshore wind. Bucket foundations benefit from the skirts, which at the cost of a minor weight increase contribute significantly to stiffness and capacity compared to surface foundations, but only a minor weight increase [12–14].

Bucket foundations can be used in two different structural configurations to support OWTs. The different configurations,

* Corresponding author. Norwegian Geotechnical Institute, NGI, P.O. Box. 3930, Ullevål Stadion, N-0806 Oslo, Norway.
E-mail address: kristoffer.skau@ngi.no (K.S. Skau).

https://doi.org/10.1016/j.marstruc.2018.01.011
Received 20 June 2017; Received in revised form 23 January 2018; Accepted 26 January 2018

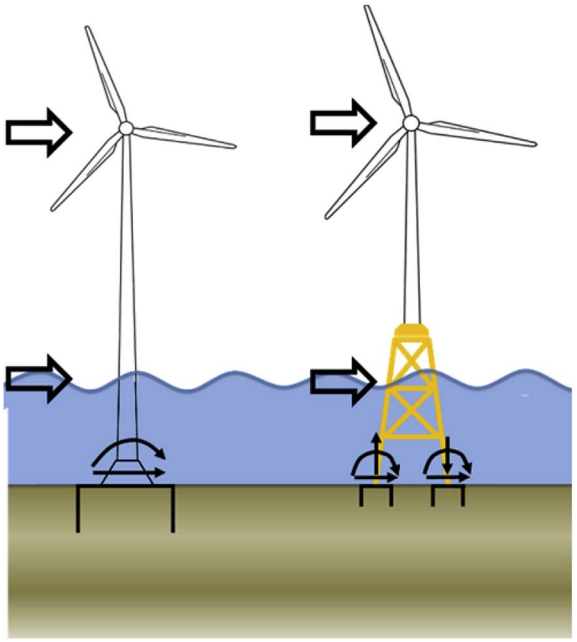

Fig. 1. Skirted foundations (buckets) supporting a) a mono tower and b) a jacket.

illustrated in Fig. 1, largely affect the loads applied to the single foundations:

a) A mono-bucket supporting a mono-tower. In this configuration, the large overturning moment from the OWT is transferred directly to the bucket as moment load.
b) Three or four buckets supporting a jacket structure. The jacket transfers the large overturning moment to the buckets though vertical load pairs.

The macro-element presented herein has been developed for modelling of bucket foundations in both configurations, thus relevant for all load combinations. Both concepts have been demonstrated as foundation method for wind turbines. A monobucket was used for an wind turbine foundation in a shallow lake in Denmark since 2002 [9] and a suction bucket jacket supporting an OWT was installed in 2014 offshore Germany [15].

A viable approach for representing bucket foundations in dynamic integrated design analyses is to model the foundation response by a macro-element. Macro-elements account for nonlinear soil behaviour in the integrated soil-structure analyses with moderate increase in the computational cost. They describe the foundation behaviour in a single point, typically with 3 (in-plane) or 6 degrees of freedom (DOF). The macro-element concept has its roots back to the pioneering work of Roscoe and Schofield [16], but development of macro-elements dedicated for integrated structural analysis accelerated in the 1990s. In the early years, the development focused on flat footings, but it became gradually more application oriented focusing in particular on spudcan behaviour for jack-ups. Along with the development of offshore wind over the last two decades, research has also focused on modelling of bucket foundation response for OWT applications [11,17–20]. These models have build on formulations developed for surface foundations and spudcans, since the overall framework suits shallow foundation behaviour in general. The difference between macro-elements for bucket foundations and those for surface foundations and spudcans are mainly the input parameters and the inclusion of tension loading. The behaviour under tension load is especially important for undrained conditions where passive suction develop under the bucket lid. Table 1 gives a brief list of some selected references considering macro-element modelling dedicated to bucket foundation and OWT application.

The most relevant macro-elements for design analyses of OWTs are the macro-elements accounting for cyclic behaviour. The

Table 1
Macro-elements representing bucket foundations for OWT application.

Model and reference	Description
Byrne (2000) [11]	Model formulations and parameters for numerical modelling presented based on experimental study on sand and clay.
Villalobos (2006) [18]	Model formulations and parameters for numerical modelling presented based on experimental study on sand and clay.
Nguyen-Sy (2007) [19]	Macro-element developed within the hyperplasticity framework. Based on the work by Refs. [11,18]
Ibsen et al., 2014 [17]	Macro-element developed within the elasto-plasticity framework. Only monotonic loading considered.
Foglia et al., 2015 [25]	Macro-element developed within the bounding surface framework. Consider cyclic loading.

cyclic response of foundations deviate from the behaviour predicted by macro-elements developed for monotonic loading. The macro-element by Nguyen-Sy [21], which was developed in the hyperplasticity framework for bucket foundations for OWTs consider cyclic loading, hence it is most relevant in this context. The input parameters to the macro-element are determined based on physical model testing. Tables of this input can be found in Refs. [11,18,19] for conditions considered in the physical tests. Macro-elements developed for other applications than for OWTs, and within different theoretical framework, e.g. the macro-elements for surface foundations in the framework of multi-surface plasticity [22], hypo-plasticity [23] and bounding surface-plasticity [24,25], may also be used for bucket foundation modelling by appropriate calibration of model parameters, and by modifying the yield surface criteria in tension. However, a general problem with all these mention macro-elements is the lack of published methodologies describing how the macro-elements can be adapted to different ground conditions. The input parameters available in the literature do not cover the natural variation of ground conditions, and it is not obvious how to interpolate between the available parameters to conditions at hand. If new analyses or model tests have to be carried out with site specific conditions, the required number of analyses are extensive and somewhat poorly defined. This problem reflects that most of the research has focused on the theoretical formulation rather than usage, and that model accuracy for idealized conditions has been the focus rather than approximations for realistic and variable soil conditions. This may explain why macro-elements are still seldom used by practitioners in design of offshore structures. Ground conditions vary between wind farms and even within a wind farm, and the lack of literature describing how macro-elements can be adapted to real ground conditions represents a technology gap in engineering and prevent usage in design work.

The macro-element proposed in this paper addresses this need through a practically oriented formulation. It has been developed for dynamic integrated time domain analyses and consider cyclic loading including soil damping. The macro-element has been based on results from numerical analyses of foundation response in clay, considering different foundation geometries and soil profiles [26]. A key finding from this numerical study is the attractiveness of identifying a representative decoupling point and using the foundation response from pure vertical, horizontal, and moment loading of this point to compute the response to combined load paths. These principles are included in the formulation of the proposed macro-element, giving a simple yield function and a site specific anisotropic hardening. These formulations make the model adaptable to different layered clay profiles and foundation geometries. The input parameters are physical and derivable in design through conventional geotechnical analyses.

The paper is divided into three main parts. Section 1 reviews the bucket foundation concept, its application within offshore wind and some aspects of existing macro-elements. Sections 2, 3 and 4 present an example of foundation response, its implications for the macro-element formulation, and most importantly the actual formulation and the required input data. Section 5 shows the performance of the macro-element by three examples.

2. Basis for the proposed macro-element formulation

2.1. Definitions and nomenclature

The paper presents loads and displacements variables in the form of energy conjugates. The moment is divided and the rotation is multiplied by the factor $D/2$, where D is the foundation diameter. This gives values roughly in same range for all DOF, making plotting and comparison convenient. The nomenclature are shown in Fig. 2a, and the load and displacement vectors are written:

$$\boldsymbol{F} = \begin{bmatrix} V \\ H \\ 2M/D \end{bmatrix}, \quad \boldsymbol{u} = \begin{bmatrix} u_v \\ u_h \\ u_\theta \cdot D/2 \end{bmatrix} \tag{1}$$

The foundation's load-displacement response is shown in a load reference point (*LRP*), defined below seabed at a depth $z = z_{LRP}$. The depth is defined by the foundation's rotation point during moment loading. This point is case specific and given by ratio between the foundation horizontal displacement at seabed $u_{h,seabed}$ and the foundation rotation u_θ:

$$z_{LRP} = \frac{u_{h,seabed}}{u_\theta} \tag{2}$$

Fig. 2b illustrates the physical interpretation of z_{LRP}, which can be described as: *the depth where negligible horizontal displacement evolves when a moment load is applied to the foundation*. As seen from equation (2), z_{LRP} contains information about the coupling between the horizontal displacement and the rotation of the foundation. In other words it reveals an important foundation characteristic. It will be shown later that z_{LRP} varies depending on the load level. However, the variation is moderate and it is possible to

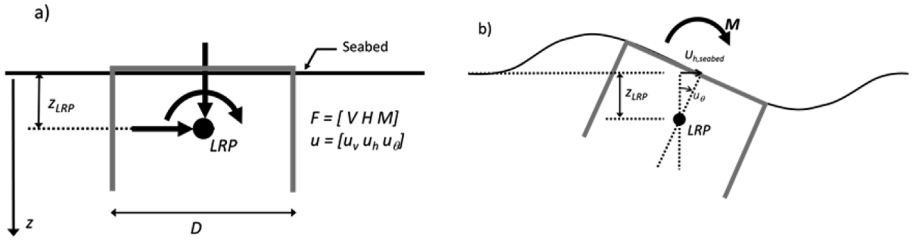

Fig. 2. a) Definition of load vector and displacement vector, b) Physical interpretation of the load reference point LRP.

define a representative value for a given case. The variation of z_{LRP} has been studied in Refs. [11,18,27], mainly focusing on the effect of foundation aspect ratio (D/h) for bucket foundations in sand. However, z_{LRP} is also a function of the soil profile. Different layering and different soil types will impose different soil reactions on the bucket foundation. Due to the non-constant nature of the *LRP*, readers may find it a confusing reference. However, it has deliberately been chosen to illustrate a fundamental ingredient in the formulation of the macro-element. This is further explained in Chapter 5, which presents the macro element formulation and elaborate on the role of z_{LRP} in the formulation.

2.2. FE-model

The ground conditions in offshore wind farm sites vary extensively and no sensitivity study can cover all natural variations. However, a wide range of profiles and bucket geometries, was considered in Ref. [26] by a series of three-dimensional (3D) finite element analyses (FEA). The commercially available software PLAXIS 3D [28] was used for the numerical study. The results from these analyses formed the "experimental" basis for the macro element development. The 3D FEA in PLAXIS considered a skirted foundation with diameter (D) and skirt penetration depth (h). One of the cases considered in Ref. [26] is presented herein to illustrate some of the fundamental characteristics of bucket foundation response and specifically the consequences for the macro-element formulation.

The soil model used in the analyses was the NGI-ADP model [29]. The NGI-ADP model describes undrained incompressible soil and has an anisotropic undrained shear strength failure criterion. The non-linear shear stress - shear strain response starts with the small strain stiffness $G_{\max}$ and depends further on the applied stress path according to the anisotropic formulation. The side boundaries were located at least a distance 6D away from the foundation periphery and the bottom boundary was located at a minimum distance of 6D below seabed. The soil plug inside the skirts was modelled either rigid or flexible in the numerical study of foundation response. In the case considered in this chapter, the soil plug inside the skirt was assumed to be rigid. However, analyses and results included in chapter 6, consider both assumptions. The mesh was refined around the skirt tip to avoid artificial stress concentrations at skirt tip and reduce the potential for overshoot in the analyses as explained in Ref. [30]. Interface elements were used between the soil and the structure. The mesh quality was assessed by comparing the capacity at vertical failure with the result from a 2D axisymmetric model with very fine mesh discretization. The overshoot was less than 5% at failure and considered to be sufficient for the purpose of this study. The strength in the interface was reduced to half of the value in the soil to account for installation effects in over-consolidated clay, similar to the assumption in Ref. [26]. Fig. 3 shows the FE-model.

The static undrained shear strength in this FEA increased linearly with depth. Expressed through the direct simple shear strength (s_u^{DSS}) [31], the linear increase was $ds_u^{DSS}/dz = 7$ kPa/m. The stress - strain behavior is taken from the NGI-database on cyclic behavior of clays, represented an over-consolidated clay typical for North Sea offshore wind farm sites. Data for Drammen clay $OCR = 4$, subjected to 10 perfectly symmetric cyclic amplitudes (average load equal zero, $F_a = 0$, and number of cycles, $N = 10$). Reference is made to [32] for a general introduction to the NGI-approach to cyclic loading, including laboratory testing and the applications in offshore foundation design. The procedure's applicability to offshore wind turbines is discussed in Ref. [33], and the determination of the specific curves used in the FEA is explained in Ref. [26]. However, the stress - strain curve used in these analyses should only be considered as an example. The loads and displacements from these analyses are evaluated in the load reference point (*LPR*) at a depth, $z_{LRP} = 2h/3$. The foundation has a diameter $D = 10$ m and $h/D = 1$. The case is later introduced as example A (Fig. 7a).

2.3. FEA results - development of plastic deformation

The foundation displacement is divided into an elastic and a plastic part in line with elasto-plastic theory from soil mechanics ($d\boldsymbol{u} = d\boldsymbol{u}^e + d\boldsymbol{u}^p$). Plastic displacement gradually evolve when the mobilization level increases. In the context of a macro-element formulation, it is useful to examine the evolving plastic work, since it reveals information about the plastic flow direction. The incremental plastic work is expressed as:

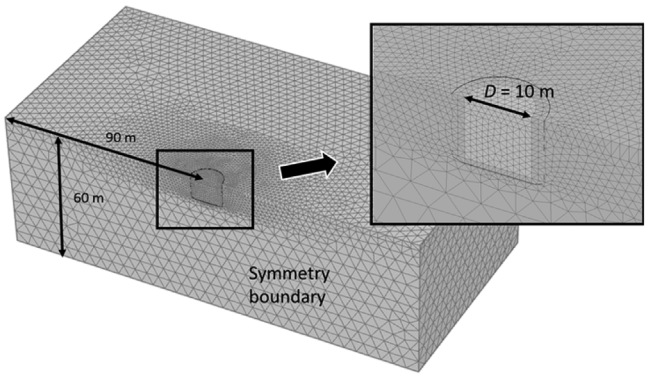

Fig. 3. 3D FEA model.

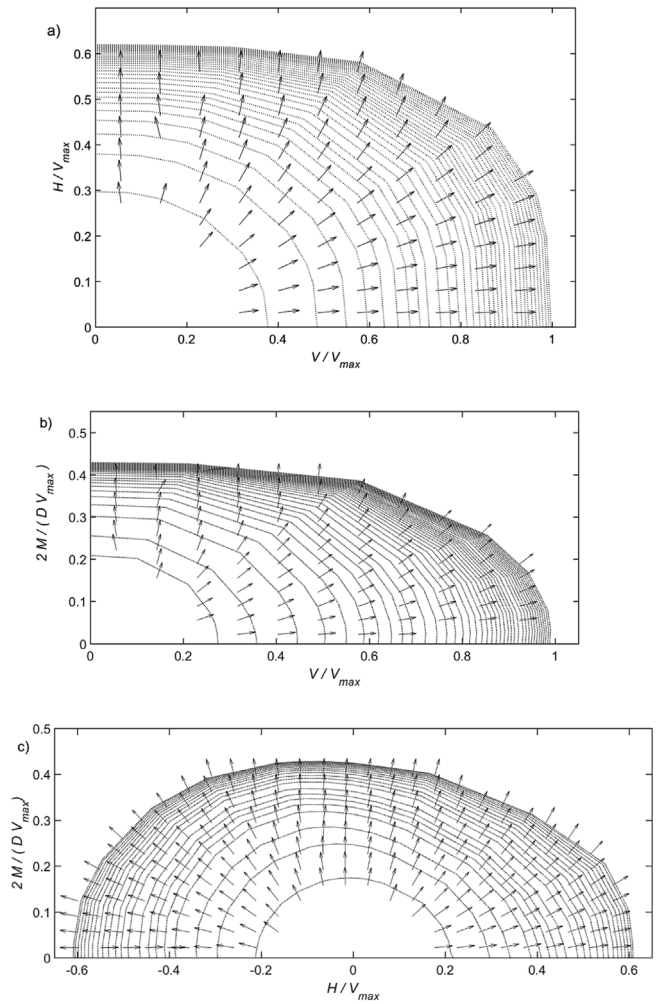

Fig. 4. Contours of plastic work, W^p and arrows pointing in the direction of the plastic flow from 3D FEA in the three load planes: a) HV-, b) HM- and c) VM-plane.

$$dW^p = \boldsymbol{F}^{\boldsymbol{T}} \cdot d\boldsymbol{u}^{\boldsymbol{p}} = (V \cdot du_v^p + H \cdot du_h^p + M \cdot du_\theta^p) \tag{3}$$

and the relation to plastic flow can be shown by the partial derivate of W^p:

$$\partial W^p / \partial \boldsymbol{F} = [du_v^p \quad du_h^p \quad du_\theta^p] \tag{4}$$

Fig. 4 shows evolving plastic work computed in FEA. The figure shows contour lines of W^p in the three normalized load planes *VH*, *VM* and *HM* with the out of plane load equal zero. The arrows in the figure are computed plastic flow vectors. As expected, the arrows are oriented perpendicular to the contours of W^p (surface normals), and this will be utilized later in the macro-element formulation.

It is clear that the contours of W^p do not have the same shape for all levels of mobilization. This is easily seen by inspecting where the contours cross the axes. The ratios between these values are not similar for all contours. For example, the contours along the normalized H-axis are more densely spaced than along the V-axis. In can also be seen that the contour lines have the shape of an ellipse at low mobilization. For higher mobilization, the shape gradually changes. Note that the contours shown in Fig. 4 are only examples, since the contours will depend on stratigraphy and soil behaviour on a specific site. However, they reveal a very important fundamental characteristic that should be addressed by a macro-element:

- The plastic work evolve non-proportional along the three load axes.
- The plastic flow direction changes not only by load path direction, but also by mobilization level.

Section 3.4, considering yield surface and flow rule, elaborate more on the consequence of these observation for the macro-element formulation.

3. Model formulation

3.1. Multi-surface plasticity

The macro-element is formulated within the framework of multi-surface plasticity. The multi-surface plasticity approach was developed in the 1950s and 1960s motivated by the need for describing behaviour of metals when subjected to cyclic loading [34–36]. The attractiveness of the concept comes from the easy implementation of kinematic hardening, which make the macro-element exhibit hysteretic behaviour. Several models have also been suggested for soil based on multi-surface plasticity [37–39]. The multi-surface plasticity approach has also been successfully applied for macro-elements of foundations. Ngyen-Sy proposed a multi-surface macro-element for suction caissons based on the hyperplasticity theory [19] and Cremer proposed a macro-element for shallow foundations [22] adapted from the multi-surface plasticity model for soils by Prevost [38]. The multi-surface plasticity models consist of several surfaces which can be translated in the load (or stress) space. The innermost surface encircle the elastic domain. When the load point moves around in the load space, it may violate the surfaces. These surfaces will be translated according to the movement of the load point. The surface translation will generate plastic displacement. Fig. 5 illustrates the principle. The figure shows a 2D-load space where a load point moves from point A to E through the following steps:

A to B The load point violates no surface and the response is elastic.

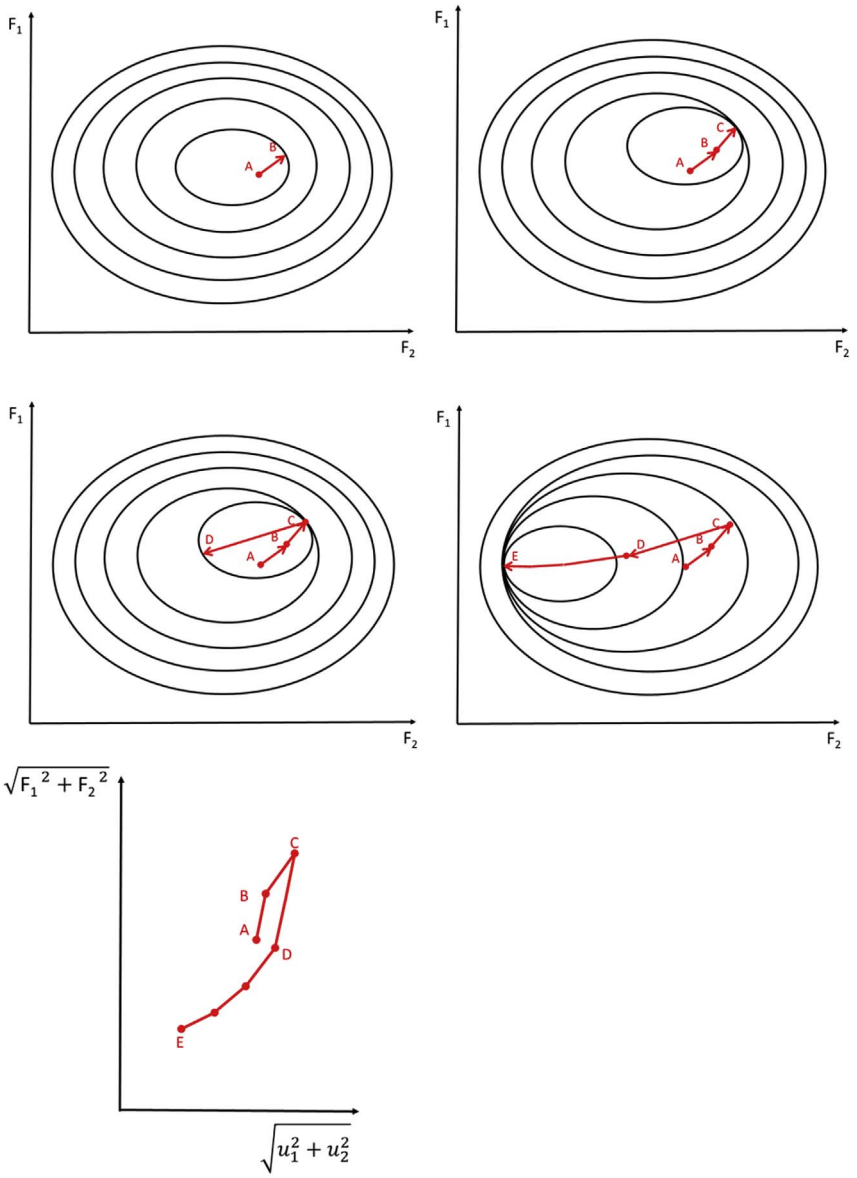

Fig. 5. Illustration of the multi-surface plasticity principle with translation of yield surfaces in the F_1 - F_t load space.

B to C The load increases and the first yield surface is violated and pulled (translated) along with the load point. The translation of the surface gives a plastic contribution to the response.

C to D The load path is reversed, and none of the surfaces are violated. They do not translate and the response is again elastic.

D to E The load point violates surface after surface, and the increasing number of surfaces translating will give increasing plastic contributions to the total response.

If the surfaces do not change in size, the model will exhibit pure kinematic hardening, and the origin of the surfaces will serve as a memory of the latest cyclic history. In this macro-element formulation, it was chosen to make the outer-most surface to a bounding surface which do not translate, thus representing an outer limit load state.

3.2. Macro-element limitations and simplifications

The macro-element is intended for dynamic integrated analyses of OWT. The model does not consider accumulation of displacement and degradation of stiffness as function of load cycles. The simplifications were chosen for several reasons. Firstly, estimates on accumulations such as tilt etc. are addressed outside integrated dynamic analyses. Secondly, the estimates of stiffness degradation and especially accumulation are very challenging. Time domain approaches are generally unreliable for such high number of load cycles. Explicit approaches [40–42] are better suited for such long-term estimates. Thirdly, the period considered in an integrated OWT analysis is typically 10 min. The stiffness degradation and accumulation of displacement during this short period is negligible for the load range relevant for OWT. Degradation may rather be accounted for prior to the analyses, when the input is defined, e.g. by the procedure proposed in Ref. [26]. In line with this approach pore pressure accumulation and mean stress changes are not computed internally in the model.

The macro-element has been developed based on foundation behaviour in clay. However, it may also give reasonable results for sand. As shown and discussed in Refs. [33,43], the stress-strain response in sand and clay are not so fundamentally different if the sand response is predominately undrained during a single cycle and if the loads are relatively small, such that no significant pore-pressure accumulation occur. Both conditions will often be present for an offshore wind bucket foundation in sand, as indicated in the field measurement of the full scale prototype suction bucket jacket at the Borkum Riffgrund 2 windfarm [15]. However, more research is required to evaluate the accuracy of the macro element representing bucket foundations in sand.

Since user friendliness has been emphasized in the development, accuracy has been compromised on the benefit of simplicity in the formulation and a limitation of number of input parameters. The mathematical functions in the formulation have been defined without non-physical empirical calibration factors. Such factors could have increased the accuracy, but reduced the user availability.

It was also chosen to ignore effects that may dominate high frequency loading and oscillation as inertia effects, radiation damping and load rate effects.

3.3. The role of the load reference point, LRP

Most macro-elements are formulated with displacements and loads located at an *LRP* at seabed. The proposed model is different and operates with the depth of the *LRP* as an input (z_{LRP}). The determination and the physical interpretation of z_{LRP} is already explained by Equation (2) and shown in Fig. 2. The elasto-plastic formulation uses the *LRP* as a reference, but the interface between the structure and the foundation can be defined in any point, e.g. at seabed. The load and displacement is transferred by a linear transformation matrix to the depth of *LRP*. This approach of a z_{LRP} different from seabed may seem unnecessarily complex and cumbersome. However, it brings some convenience for the macro-element formulation. Firstly, the mathematical functions become simpler. Secondly, z_{LRP} store information about the coupling between the horizontal displacement and rotation, and quantify this coupling by a physical interpretable parameter. Section 5.5 elaborate on these conveniences in the discussion on yield surface and flow rule.

It is important to realize that the parameter z_{LRP} cannot be a general/hardcoded value but a case specific input parameter, which makes the macro-element adaptable to different site conditions and foundation geometries. Since z_{LRP} is dependent on the mobilization level, an approximate representative value has to be chosen. Chapter 6, which consider the macro-element input will elaborate more on the determination of a representative z_{LRP}, and discuss the assessment of the error imposed by the assumption.

3.4. The elastic stiffness matrix

The elastic stiffness matrix is defined as a 3 × 3 matrix:

$$\boldsymbol{D} = \begin{bmatrix} k_v^e & 0 & 0 \\ 0 & k_h^e & 0 \\ 0 & 0 & k_\theta^e \end{bmatrix} \tag{5}$$

The stiffness coefficients k_v^e, k_h^e and k_θ^e refer to the elastic stiffness in the vertical direction, horizontal direction and rotation around the out of plane axis. The coupling terms are set to zero since the *LRP* is located below mudline and implicitly includes parts of the coupling between the horizontal load and moment applied at seabed. This is an approximation, and it will be shown later that z_{LRP} varies as function of the mobilization level.

3.5. Yield function and flow rule

The yield function and the flow rule are formulated based on the FEA results as those shown earlier in the paper. As stated initially, it is an aim to formulate the macro-element mathematically transparent and simple. For low mobilization levels, Fig. 5 shows that the contours of plastic work where reasonably approximated by elliptic surfaces. The macro-element is intended for OWT foundations, where low and moderate mobilization levels are most relevant. An elliptic surface is therefore taken as the potential function, g. It was also chosen to use these surfaces as yield surfaces. The yield function f is then given by the same function imposing associated flow, for all surfaces i :

$$\frac{\partial g_i}{\partial \boldsymbol{F}} = \frac{\partial f_i}{\partial \boldsymbol{F}} \tag{6}$$

where f_i is an ellipsoid:

$$f_i = \left(\frac{V - \alpha_{i,V}}{V_{i,max}}\right)^2 + \left(\frac{H - \alpha_{i,H}}{H_{i,max}}\right)^2 + \left(\frac{M - \alpha_{i,M}}{M_{i,max}}\right)^2 - 1 \tag{7}$$

The denominators $V_{i,max}$, $H_{i,max}$ and $M_{i,max}$ are the axis crossings for the surface i . $\alpha_{i,V}$, $\alpha_{i,H}$, $\alpha_{i,M}$ are the coordinates of the origin (initially equal zero) of surface i . Compared to other yield surface formulations [44–46], the function cannot describe rotated ellipses. However, this is accounted for by keeping the depth of the load reference point (z_{LRP}) as an input. This will effectively describe the same response at seabed. The values of $V_{i,max}$, $H_{i,max}$ and $M_{i,max}$ will determine the shape of the ellipses, thus the flow direction. The values should therefore be determined based on the development of plastic work along the three axes.

3.6. Surface translation and hardening rule

The surface translation rule normally refers to the rule dictating the direction of translation of the surfaces. A widely used approach is to determine the direction based on an image point located on an image surface. This image surface can be the “next surface outside” as propsed by Mrótz [37,47] or the outermost bounding surface [38,48]. The image point is typically defined by requiring the surface normal vector on the image surface to be equal (parallel) to the surface normal vector of the “active” surface at the load point. The “active” surface is typically the last violated surface or the inner-most elastic surface in bounding surface models. These relatively complicated rules are motivated by the overall preference of the so called “non-intersection surface criteria”. This criteria has been considered to be convenient and by some even necessary. However, there is no clear evidence or explanation available in the public domain that can underpin this requirement [49]. Some may still find the non-intersection criteria to be convenient. But as showed by Montáns and Caminero [50] in their thorough examination of these types of surface translation rules, they can lead to accumulation of displacements (model drift). Such displacement accumulation can impose significant forces in analyses of multi-leg structures. In earlier versions of this macro-element, such drift problems were encountered when a Mrótz-type translation rule [37,47] was applied. In light of the above discussion, it was decided to formulate the surface translation without any restrictions from surrounding surfaces. The surface translation is then determined by a relatively simple hardening rule controlling the relation between surface translation and plastic displacement. The hardening is a multilinear approximation. This means that each surface, i has a constant “plastic stiffness”. The total plastic displacement is taken as sum of all plastic displacement contributions using the Koiter rule [51]:

$$d\boldsymbol{u^p} = \sum_{i=1}^{k} d\boldsymbol{u_i^p} = \sum_{i=1}^{k} d\lambda_i . \partial g_i \big/ \partial \boldsymbol{F} \tag{8}$$

where k is the outermost surface being violated. Since the foundation response is anisotropic by nature, an anisotropic hardening formulation has been adapted. The hardening is based on the load – displacement response in the three uniaxial directions. The approach of using the three uniaxial responses as basis for describing general response to any load path, was illustrated in Skau et al. [26]. In this formulation, the hardening for a combined load path is approximated by weighting the plastic stiffness in the three uniaxial directions by the flow direction for the current load state. The formulation, also used for modelling clay in Ref. [52], can be expressed for any surface i as:

$$\partial \boldsymbol{\alpha_i} \big/ \partial \lambda_i = \boldsymbol{D}_i^p . \partial g_i \big/ \partial \boldsymbol{F} \tag{9}$$

where $\partial g_i \big/ \partial \boldsymbol{F}$ is the plastic flow direction vector, and $\boldsymbol{D}_i^p$ is the “plastic stiffness matrix” for surface, i :

$$\boldsymbol{D}_i^p = \begin{bmatrix} k_{i,v}^p & 0 & 0 \\ 0 & k_{i,h}^p & 0 \\ 0 & 0 & k_{i,u\theta}^p \end{bmatrix} \tag{10}$$

$k_{i,v}^p$, $k_{i,h}^p$, $k_{i,u\theta}^p$ refer to the plastic stiffness in the vertical direction, horizontal direction and rotation around the out of plane axis. Note that the plastic stiffness, $\boldsymbol{D}_i^p$, is only associated with the translation of surface i . This means that e.g. the vertical tangential stiffness $K_{k,v}^p$, for loading between $V_{k,max}$ and $V_{k+1,max}$ is the combined stiffness from all surfaces being translated. This is analogue to the total stiffness of 1D-springs coupled in series:

$$\frac{1}{K_{k,v}^{p}} = \sum_{i=1}^{k} \frac{1}{k_{i,v}^{p}} \tag{11}$$

3.7. Numerical implementation

The model was formulated such that it always find the solution with translation of as few surfaces as possible. This is achieved simply by a loop starting with the inner-most surface, $i = 1$. When the convergence criteria has been met, the routine checks whether the next surface $i = 2$ has been violated. If so, a new solution is found with surface 1 and 2. This goes on until a solution is found involving translation of all surfaces i from 1 to k while the next surface, $k + 1$, is not violated. This means that every increment is a multi-yield criteria problem, which gives the elasto-plastic relation for k surfaces:

$$d\boldsymbol{F} = \boldsymbol{D}\cdot\left(d\boldsymbol{u} - d\lambda_1\frac{\partial g_1}{\partial \boldsymbol{F}} - d\lambda_2\frac{\partial g_2}{\partial \boldsymbol{F}} - \ldots - d\lambda_k\frac{\partial g_k}{\partial \boldsymbol{F}}\right) = \boldsymbol{D}\cdot\left(d\boldsymbol{u} - \sum_{i=1}^{k} d\lambda_i \cdot {\partial g_i}\Big/{\partial \boldsymbol{F}}\right) \tag{12}$$

By utilizing the consistency condition, a system of equations with k unknown is established:

$$\begin{bmatrix} f_1 \\ f_2 \\ \vdots \\ f_i \\ \vdots \\ f_k \end{bmatrix} = \begin{bmatrix} (A_2 + a_{22}) & a_{12} & \ldots & a_{1,j} & \ldots & a_{1k} \\ a_{21} & (A_1 + a_{11}) & \ldots & a_{2,j} & \ldots & a_{2k} \\ \vdots & \vdots & \ddots & \vdots & \ldots & \vdots \\ a_{i,1} & a_{i,2} & \ldots & a_{i,j} & \ldots & a_{k,j} \\ \vdots & \vdots & \ldots & \vdots & \ddots & \vdots \\ a_{k1} & a_{k2} & \ldots & a_{kj} & \ldots & A_k + a_{kk} \end{bmatrix} \cdot \begin{bmatrix} d\lambda_1 \\ d\lambda_2 \\ \vdots \\ d\lambda_i \\ \vdots \\ d\lambda_k \end{bmatrix} \tag{13}$$

where

$$a_{i,j} = \frac{\partial f_i}{\partial \boldsymbol{F}}^{T} \boldsymbol{D} \frac{\partial g_j}{\partial \boldsymbol{F}} \text{ and } A_i = \frac{\partial f_i}{\partial \boldsymbol{F}}^{T} \boldsymbol{D}_i^{p} \frac{\partial g_i}{\partial \boldsymbol{F}} \tag{14}$$

The details in the derivation of eq. (13) are shown in Appendix A. The publicly available LAPACK Fortran routines solves this system of equations in eq. (13). The complete macro-element has also been written in Fortran and is about to be implemented in the aero-hydro-servo-elastic code 3D float [53].

4. Macro-element input

The input has been limited to ensure simplicity for users. With the exception of numerical parameters such as tolerance and number of substeps, the input is limited to:

- The depth of the load reference point, z_{LRP}. The depth where negligible horizontal displacement evolves when a moment load is applied to the foundation.
- The uniaxial response – for loads applied in the load reference point. In total three curves $V - u_v$, $H - u_h$, M - u_θ, as tabulated data.
- Number of surfaces, N

Fig. 6 illustrates this input. Only one FEA is required to compute the depth to the load reference point, z_{LRP}. It will be shown later that z_{LRP} varies as function of mobilization, and it should be verified that the variation is a within an acceptable range for the load range of interest. Based on simplified sensitivity studies, it was found that 10% difference in z_{LRP} gave 12% difference in the moment load. However, the effect is influenced by the ratio between the horizontal and rotational stiffness, and sensitivity checks should be

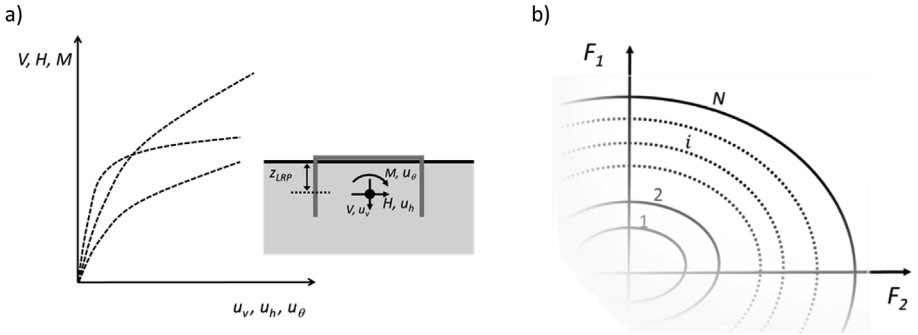

Fig. 6. Illustration of the required model input: a) Depth to load reference point, z_{LRP}, and the uniaxial load-displacement response for the reference point b) Number of surfaces.

carried out for the problem under consideration.

Due to large variations in soil conditions offshore, it is of great importance that the uniaxial input response curves are site specific. A pre-defined hardening would not be able to represent the foundation response well. The uniaxial input response curves are used as back-bone curves. This means that the uniaxial input response curves should reflect the foundation's cyclic behaviour. The authors recommend to use FEA to establish the uniaxial response curves. The analyses can be run as quasi static analyses, but the soil's stress –strain curve should reflect a cyclic backbone curve. If laboratory data is available, these can be used directly to extract cyclic behaviour. The effect of cyclic degradation can be accounted for directly by defining the appropriate stress-strain curves.

If the uniaxial load displacement curves are based upon monotonic soil data, the effect of cyclic degradation on foundation level can be approximated by the data in Skau et al. [26] or similar. However, care should be taken regarding the damping produced by the macro-element. The macro-element include material (hysteretic) damping, while radiation damping is ignored. The damping produced by the macro-element will follow Masing's rule with the three input curves as basis. This means that the assessment should be based on one of the following:

1) *On stress-strain level* - by assuming Masing's rule for the stress-strain curves (used in the FEA providing uniaxial input), the damping on stress strain level can be computed. These levels can be compared with damping computed from laboratory stress-strain loops. If no such cyclic laboratory data exist, strain-damping relations proposed in the literature e.g. by Darendeli [54] may give a good indication.
2) *On foundation level* - The global damping can be computed by FEA as demonstrated by Carswell et al. [55]. In these analyses, strain-damping relations are required. This FEA computed global damping can be compared with macro-element damping for different load paths.

It is important to make clear that the macro-element is not restricted to a specific procedure for establishing the uniaxial load-displacement data. E.g. if relevant model test data are available these can be used.

The macro-element does not use the uniaxial input response curves directly, but transfer them to a linear elastic stiffness matrix $\boldsymbol{D}$, linear "plastic stiffness matrices" $\boldsymbol{D}_i^p$ and yield function axis crossings ($V_{i,max}$, $H_{i,max,}$ $M_{i,max}$). These are determined by an automatized discretisation of the uniaxial load – displacement curves. The routine determines the shape of the ellipses (flow direction) and secondly the corresponding hardening parameters. The code has been written in Matlab but can easily be adapted to Excel or similar programs. The routine follows the steps:

1. Compute three uniaxial load - plastic work curves by numerical integration of the three load – displacement curves.
2. Discretize one load axis according to the number of surfaces, *N*. The user specify the axis. If one load direction is expected to dominate the response, it is recommended to use this load axis as basis for the discretisation. The interval between surfaces along this axis will be constant.
3. The plastic work for the *N* axis crossings along the chosen axis is found by interpolation.
4. The corresponding crossings (equal plastic work) along the two other axes are found by interpolation.
5. The elastic stiffness is computed based on the displacements relevant for the first surface at $V_{1,max}$, $H_{1,max}$, $M_{1,max}$.
6. The corresponding tangential stiffness's in the three directions is computed between the axis crossings.

In addition to the elastic stiffness matrix, the routine gives two tables of hardening input for the macro element model: $3N$ axes crossings, and $3N$ tangential stiffness's. The user will not see the stiffness coefficients for each individual surface ($\boldsymbol{D}_i^p$) since these are computed inside the macro-element routine.

5. Macro-element demonstration and back-calculation

The performance of the macro-element was demonstrated through three examples including a back-calculation of a field test:

Example A. General monotonic loading of a 10 m diameter foundation with 10 m skirts installed in clay with shear strength increasing linearly with depth.

Example B. Irregular cyclic loading of a 10 m diameter foundation with 5 m skirts installed in clay with a stiff layer from 7.5 – 17.5 m.

Example C. Back-calculation of the Bothkennar field test of a bucket foundation subjected to cyclic loading [56].

Example A is partly a verification of the macro-element, since the model's response to several load directions has been compared with the response computed in 3D FEA. Example B demonstrate the macro-element's stability with respect to numerical ratcheting (model drift). Finally, example C compare measurements from a large scale field test with computed cyclic response.

5.1. Example A - foundation response to monotonic loading

The aim of this example is to reproduce results computed by the 3D FE-model presented in section 2.2. Fig. 7a shows the case considered. The input was established by the procedure described in Section 4. The FEA response from the uniaxial moment loading were used to calculate z_{LRP}/h based on eq. (15). Fig. 8 shows the calculated z_{LRP}/h as function of the normalized load. A z_{LRP}/h value

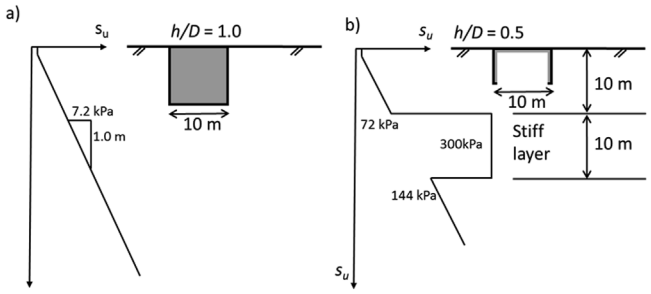

Fig. 7. Soil profiles and foundation geometry used in the model demonstrations, a) Example A, b) Example B.

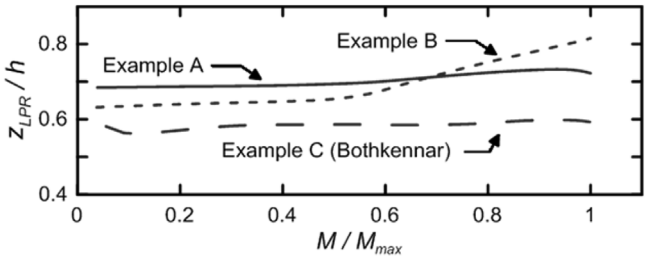

Fig. 8. Computed z_{LRP} as function of normalized load for the three examples.

of 0.67 was chosen in these analyses. The three uniaxial curves shown in Fig. 9 were computed by FEA and used as input.

Comparisons between the response computed by FEA and by the macro-element for various radial load paths are shown in Fig. 10, Fig. 11 and Fig. 12. Both the resultant values ($|F| = \sqrt{V^2 + H^2 + (2M/D)^2}$, $|u| = \sqrt{u_v^2 + u_h^2 + u_\theta^2 D/2}$), and the individual components e.g. $u_v - u_h$ are compared. The agreement between the macro-element and the FEA is generally good. The deviations are most pronounced in the *HM*-plane (Fig. 12). This is due to the simplification of the yield and potential function, which is less accurate in the *HM*-load plane (ref. the contours of plastic work in Fig. 4c). This deviation might be slightly improved by adjusting z_{LRP}. However, it cannot be completely eliminated because of the fundament non-symmetric nature of the *HM*-load plane as discussed in Skau et al. [26].

5.2. Example B - foundation response to general cyclic loading

The response to cyclic loading was demonstrated by applying a cyclic load history to a foundation with 10 m diameter and 5 m deep skirts. The bucket lid and skirts were given a very high stiffness compared to the soil such that the foundation appeared rigid in

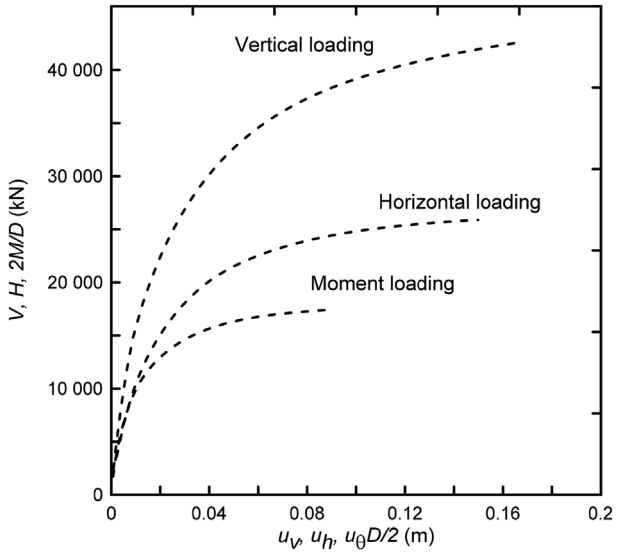

Fig. 9. Uniaxial load-displacement response for macro-element input in example A.

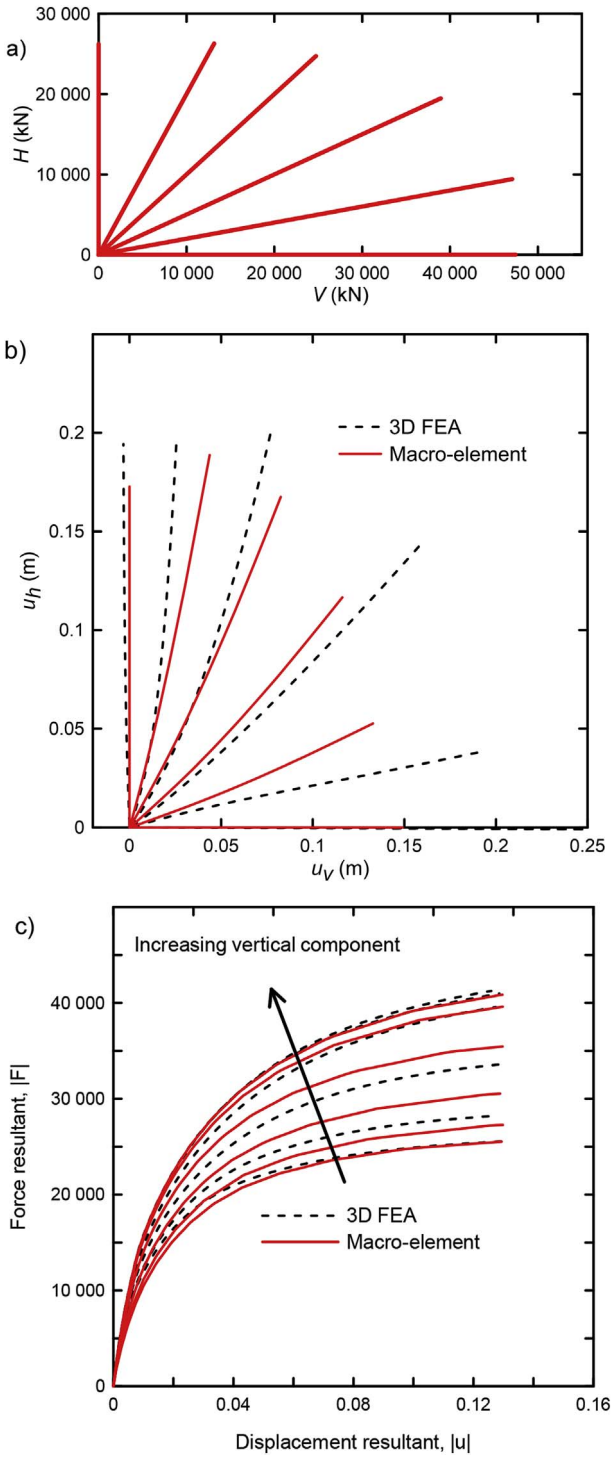

Fig. 10. *Load – displacement response in the VH-load plane (M = 0) computed by 3D FEA and the macro-element. a) VH load paths, b) u_v - u_h displacements c) Load – displacement resultant.*

the problem. The bucket had no internal stiffeners and the soil plug inside the skirts could deform. The profile had linear increasing shear strength and stiffness similar to Example A, except from a stiffer layer at 7.5 m to 17.5 m depth. The cyclic properties represented Drammen clay with $OCR = 4$, $F_a = 0$ and a cyclic degradation expressed as $N_{eq} = 10$ (similar to the cyclic properties used in Example A). The shear strength and stiffness in the "stiffer layer", were increased by a factor 2 compared to the profile in Example A. Fig. 7b) shows the soil profile.

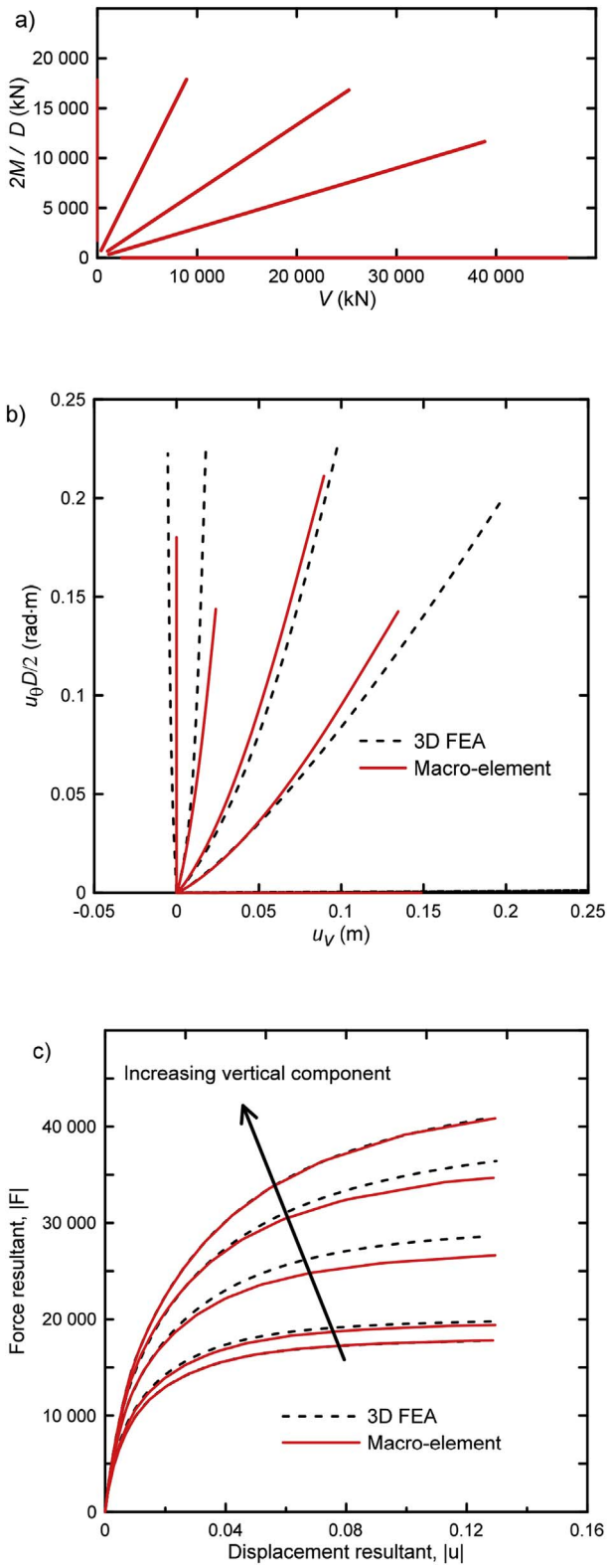

Fig. 11. Load – displacement response in the *VM*-load plane ($H = 0$) computed by 3D FEA and the macro-element. a) *VM* load paths, b) $u_v - u_\theta \cdot D/2$ displacements c) Load – displacement resultants.

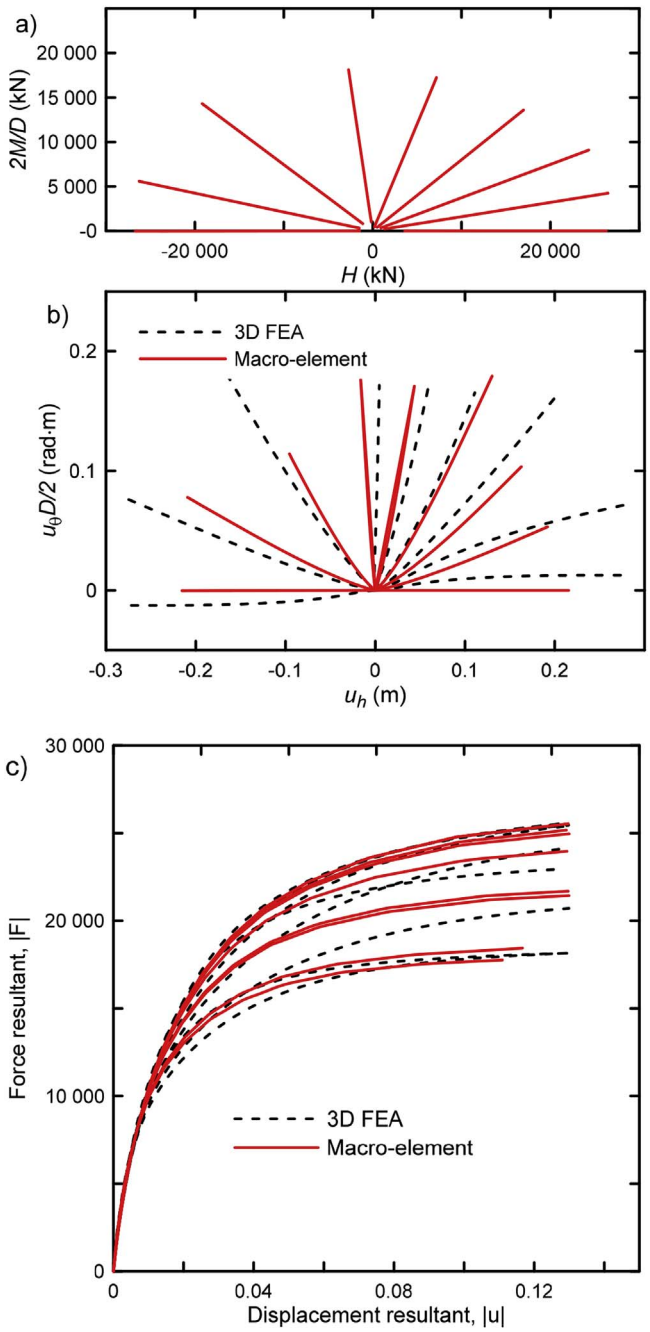

Fig. 12. Load – displacement response in the *HM*-load plane ($V = 0$) computed by 3D FEA and the macro-element. a) *HM* load paths, b) $u_h - u_\theta \cdot D/2$ displacements c) Load – displacement resultants.

The macro-element input was established by 3D FEA. The FE-model was similar to the model described in section 2.2 except the required modifications to reflect Example B. The bucket geometry was updated and the soil plug inside the skirts assigned with soil properties. The bucket lid and skirts were modelled using plate elements, and a very high stiffness. The depth to the *LRP*, was determined based on a displacement controlled FEA. The computed z_{LRP} based on the displacements from a FEA with pure moment loading is shown in Fig. 8 $z_{LRP}/h = 0.67$ was used as for Example A. The uniaxial input response were also computed by FEA.

The foundation was subjected to a combination of horizontal and moment load. A 10-min irregular load history was applied. The ratio between the moment and horizontal load, and the moment and horizontal capacity makes the load history representative for a monopod foundation during an idling case with high wind and waves. For the purpose of demonstration, it was decided to scale the load history such that the typical cyclic amplitude was approximately 50% of the foundation capacity. Fig. 13 shows the dominant components in this analysis, the moment and the computed rotation. Note that displacements did not accumulate during the

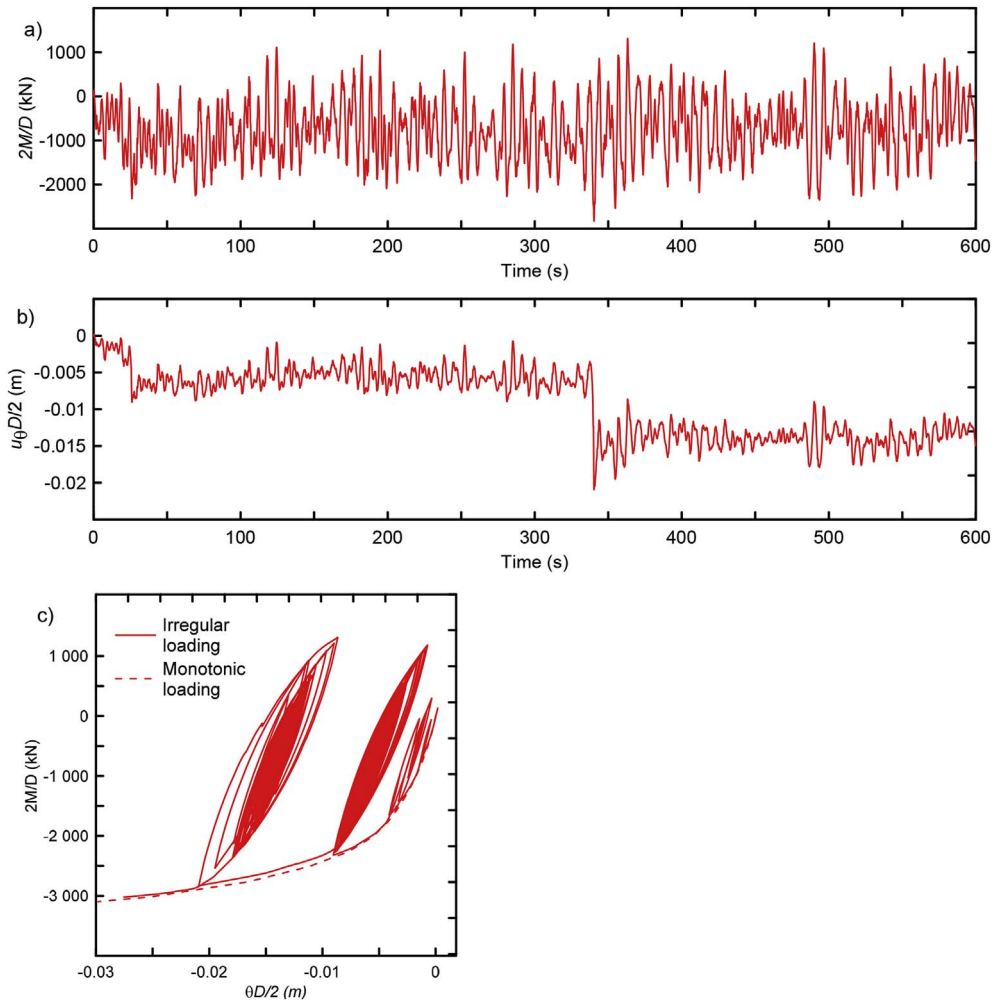

Fig. 13. Cyclic - response computed by the macro-element for example B. a) Moment - time, b) Rotation - time, c) Rotation – Moment.

simulation. The increase in rotations around 25 s and 340 s may be interpreted as accumulation, since the average displacement does not return to its previous average level even though the load history has a relatively constant average. However, this increased average displacement are in perfect agreement with kinematic hardening behaviour, and the surfaces have only temporarily been taken to a new average displacement level. At the end of the irregular history, the load was increased further making it comparable to the virgin monotonic load response (included in Fig. 13c). The figure shows that the two curves coincide.

5.3. Example C – back-calculation of the Bothkennar field test

5.3.1. Bothkennar field test

Finally, the macro element behaviour was compared with measured response from a field test of a skirted foundation in clay. The test was performed at the Bothkennar field in Scotland with a 3 m diameter foundation with 1.5 m deep skirts subjected to horizontal and moment loading. Such a load regime makes the test relevant for a monopod foundation. The test procedures and results are documented in Houlsby et al. [56]. The load applied to the foundation was grouped in three categories. Load cycles with relatively small amplitudes were first applied to the model at high frequency. The foundation response to these load cycles was significantly affected by inertia forces and of little relevance for the macro-element presented herein, which do not consider inertia forces. These load cycles were followed by the cycles being back-calculated by the macro-element. These were applied quasi-static and termed “small cycles”. The moment amplitude for these cycles was approximately 70 kNm, around 15–20% of the calculated static moment capacity. These cycles were followed by cycles of increasing amplitude giving significant degradation and accumulation of rotation after relatively few cycles. Such behaviour is not acceptable for an OWT and of less relevance for this macro-element.

5.3.2. Macro-element input

The soil condition at the Bothkennar site is documented in several papers in Geotechnique, Vol 42(2) [57]. To obtain well-defined

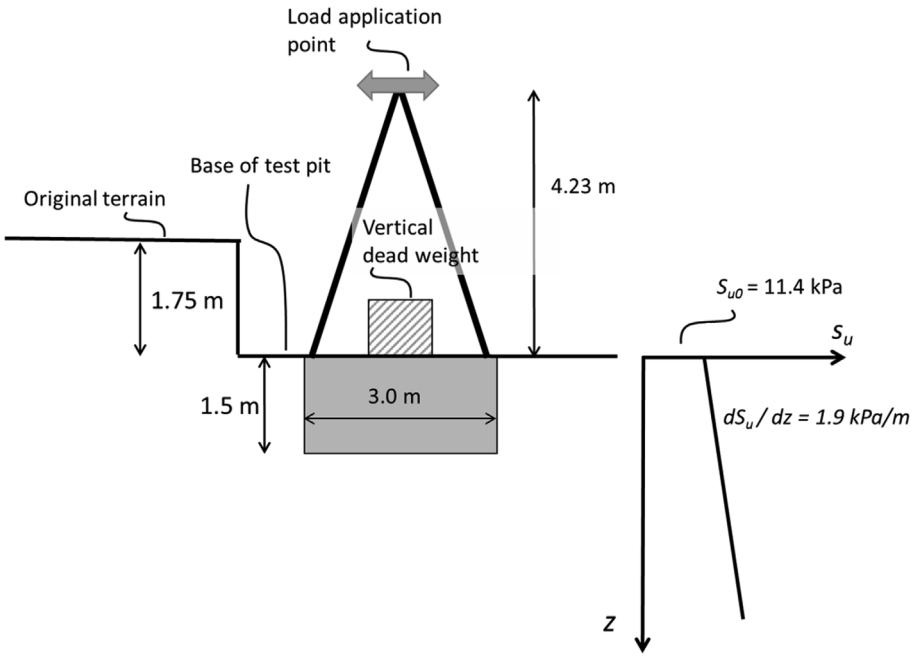

Fig. 14. *Illustration of Bothkennar field test setup and soil strength profile from* Ref. [56].

test conditions, the top soil was excavated such that only the Bothkennar clay was considered to affect the foundation response. The Bothkennar clay is a lightly over-consolidated clay, with a clay fraction of 20–40%, a water content of 50–75% and plasticity index of 30–50% [58]. Fig. 14 shows the test setup and the undrained shear strength taken from Houlsby et al. given [56] (shear strength assumed to be s_u^{DSS}). To our knowledge, no cyclic testing of the clay has been performed. This is unfortunate, since it makes it difficult to interpret the test results in light of cyclic soil behaviour on element level, which are the basis in design. Therefore, in lack of better alternatives, the cyclic stress-strain curves for the soil were based on the Drammen clay cyclic database. It was decided to use the *DSS* stress - strain data for $OCR = 4$ and $\tau_a = 0$ ($\tau_{cy}/\tau_a = 7$ in the test). $OCR = 4$ was chosen based on the increased OCR ($\backsimeq 3$) due to the excavation and the OCR profile as given in Hight et al. [58], and since the shear strength-vertical effective stress ratio (s_u/σ'_v) was in line with Drammen clay $OCR = 4$ (excavation included).

The variation in load frequency varied significantly in the first and second part of the test. The load frequency has a significant effect on the cyclic degradation and becomes less damaging when the frequency increases [32,59]. This makes it difficult to assess the degree of cyclic degradation. The stress-strain curves finally used represent $OCR = 4$, $N = 60$, accounting for the number of load cycles during the first "high frequency" testing. The part of the test that was back-calculated was carried out at a very low frequency (compared to the Drammen clay cyclic tests). The stiffness was therefore reduced by a factor 0.71, accounting for the reduce rate. The reduction reflects the difference in load rate in cyclic tests compared to standard monotonic lab tests [32,59]. A $G_{\max}/s_u^{DSS} = 500$ was used. With the soil model input established, 3D FEA were carried out to compute the depth to the load reference point and to establish the uniaxial load – displacement curves. $z_{LRP}/h = 0.59$ was used in the analyses and the computed z_{LRP} as function of normalized load is shown in Fig. 8. Fig. 15 shows the uniaxial input responses.

5.3.3. Analysis and results

The test measurements considered in this comparison did not start from zero load and displacement since load cycles were applied prior to the relevant cycles. The macro element was initiated according to this offset by applying one cycle prior to the back-calculation. This is indicated in Fig. 16a) where the applied moment load is shown. The computed and measured response are shown Fig. 16b) as function of time. Fig. 17 shows the rotation – moment response. The moment is given at the depth of the reference point. The agreement is generally good. The stiffness is in very good agreement, but the damping is somewhat underestimated by the macro-element. The agreement in the overall response means that the soil's stress-strain response used in the FEA was reasonable. However, the assumption of equivalent number of cycles (N_{eq}) of 60 based on approximately 60–70 high frequency cycles applied prior to the back-calculated cycles is questionable. Soil stress-strain response based on Drammen clay with lower N_{eq} combined with a higher OCR value, both plausible assumptions, could possibly also have given good match with the measurements. Better agreement between the measured and the computed response could have been obtained by using the measurements directly in the macro-element calibration. However, such an approach has little relevance for a design situation.

6. Extension to 5 degrees of freedom

The macro-element has been presented as a 3D macro-element in this paper. This is in line with the FEA results that have been the

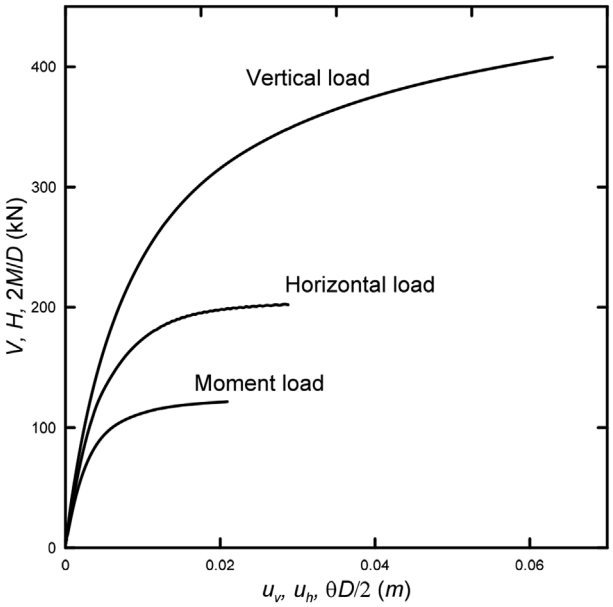

Fig. 15. Uniaxial load - displacement response for macro-element input for the Bothkennar test.

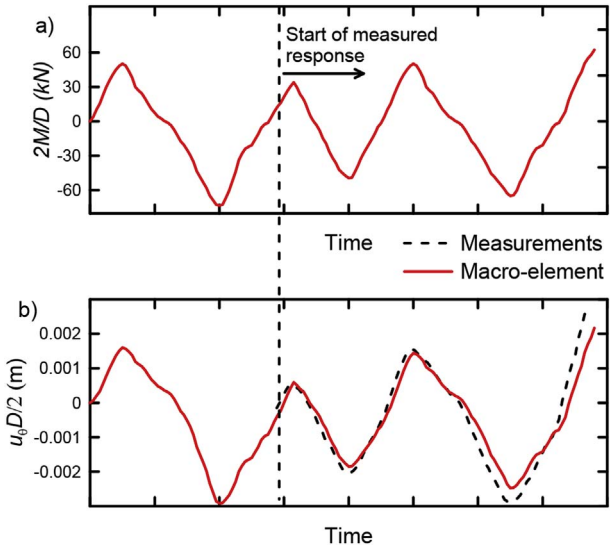

Fig. 16. Field test loading and response. a) Moment - time, b) Comparison of computed and measured rotation – time.

basis for the development. These analyses considered moment and horizontal load working in the same plane e.g. H_x and M_y (right-handed coordinate system). However, since the offshore wind turbines often face shifting wind and wave direction, there is a great need for foundation models that is somewhat more general. A first step in such an extension is to assume that the resultants remain in plane even though the load direction changes. The macro-element formulation can then be extended to five dimensions relatively easily by using the idea of the resultant load. In the horizontal x-y plane, the horizontal and moment resultant can be written:

$$H = \sqrt{H_x^2 + H_y^2}$$
$$\textit{and}$$
$$M = \sqrt{M_x^2 + M_y^2} \tag{15}$$

where H_x and H_y the horizontal load in the x and y direction and M_x and M_y is the moment around the x and y axis. The full 5-dimensional yield function can then be written:

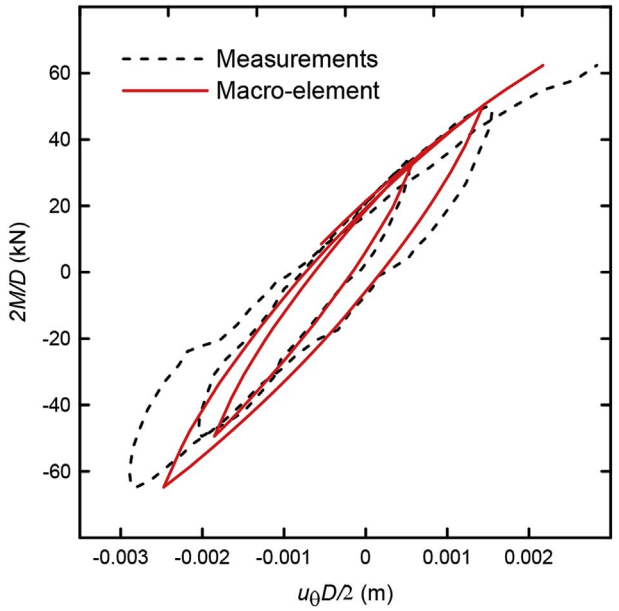

Fig. 17. Comparison of computed and measured moment - rotation response.

$$f = \left(\frac{V - \alpha_V}{V_{max}}\right)^2 + \left(\frac{H_x - \alpha_{Hx}}{H_{max}}\right)^2 + \left(\frac{H_y - \alpha_{Hy}}{H_{max}}\right)^2 + \left(\frac{M_x - \alpha_{Mx}}{M_{max}}\right)^2 + \left(\frac{M_y - \alpha_{My}}{M_{max}}\right)^2 - 1 \tag{16}$$

This is in principle similar to the extension proposed by Bienen et al. [46]. As mentioned above, there is no data in this paper that support that the formulation is correct for combination of e.g. H_x and M_x. Such a combination may dominate the loads on a mono-bucket if the wind and wave loads are misaligned. This means that the validity of the assumption is related to the angle between the resultant horizontal load and the resultant moment axis. However, the extension is a first step towards a more complete description. The extended model is implemented in the aero-elastic code 3Dfloat [53] as DLL.

7. Conclusions and further work

The paper presents a macro-element for skirted foundations in clay subjected to irregular cyclic loading. The macro-element was developed for integrated time domain analyses of offshore wind turbines. The formulation is based on the multi-surface plasticity framework and a numerical study of foundation response by FEA. The macro-element has a simple intuitive input, and was shown to reproduce, with satisfying accuracy, the response computed in FEA and the response observed in the Bothkennar field test.

The macro-element has several similarities with many of the existing macro-elements that are available in the public domain. However, there are also aspects which makes the macro-element somewhat different. The most important of these aspects are:

- All input parameters have a physical interpretation
- The use of load reference point, z_{LRP} as an input. This captures the effect of rotated elliptical surfaces in the *HM*-load plane, seen in most of the existing macro-element. The z_{LRP} depends on site conditions and bucket geometry.
- Procedures to generate input accompanies the macro-element. These procedures include FEA and make the macro-element adaptable to different soil conditions automatically updating flow directions and hardening.
- The formulation prevents numerical ratcheting.

The macro-element was developed with the purpose of being simple. Consequently, accuracy has been compromised to reduce the number of input parameters. If the macro-element is used in design, it is wise to compare the response to some general load paths computed in FEA and by the macro-element, to ensure that an acceptable accuracy is achieved.

The macro-element formulation is presented as a three-dimensional formulation in the vertical, horizontal and moment load space. However, if it is assumed that the load resultants reflect a planar load situation, an extension to 5 degrees of freedom is relatively straightforward.

Acknowledgement

The financial support by the Norwegian Research Council and the industrial partners Statoil, Vattenfall and Statkraft through project *Reducing cost of offshore wind by integrated structural and geotechnical design (REDWIN)*, Grant No. 243984, is gratefully

acknowledged. The authors would also like to thank Amir M. Kayna for his contribution, as well as the valuable comments from the reviewers.

Appendix A. Solution of multi-criteria formulations

The appendix explains the derivation of the equations when several surfaces or criteria have to be satisfied for a displacement increment. It is convenient to show this for two surfaces. The elasto-plastic relation is written:

$$d\boldsymbol{F} = \boldsymbol{D}\cdot\left(d\boldsymbol{u} - d\lambda_1\frac{\partial g_1}{\partial \boldsymbol{F}} - d\lambda_2\frac{\partial g_2}{\partial \boldsymbol{F}}\right) \tag{A1}$$

By multiplying with $\frac{\partial f_1}{\partial F}$ and combining with the consistency condition (one consistency condition for each surface):

$$\frac{\partial f_1}{\partial \boldsymbol{F}}^T\cdot d\boldsymbol{F} - A_1\cdot d\lambda_1 = 0 \tag{A2}$$

(A1) can be written:

$$\frac{\partial f_1}{\partial \boldsymbol{F}}^T d\boldsymbol{F} = \frac{\partial f_1}{\partial \boldsymbol{F}}^T \boldsymbol{D}d\boldsymbol{u} - \frac{\partial f_1}{\partial \boldsymbol{F}}^T \boldsymbol{D}d\lambda_1\frac{\partial g_1}{\partial \boldsymbol{F}} - \frac{\partial f_1}{\partial \boldsymbol{F}}^T \boldsymbol{D}d\lambda_2\frac{\partial g_2}{\partial \boldsymbol{F}} \tag{A3}$$

$$A_1\cdot d\lambda_1 = \frac{\partial f_1}{\partial \boldsymbol{F}}^T \boldsymbol{D}d\boldsymbol{u} - \frac{\partial f_1}{\partial \boldsymbol{F}}^T \boldsymbol{D}d\lambda_1\frac{\partial g_1}{\partial \boldsymbol{F}} - \frac{\partial f_1}{\partial \boldsymbol{F}}^T \boldsymbol{D}d\lambda_2\frac{\partial g_2}{\partial \boldsymbol{F}} \tag{A4}$$

The expression can be simplified by introducing $a_{11},\ a_{12}$:

$$a_{11} = \frac{\partial f_1}{\partial \boldsymbol{F}}^T \boldsymbol{D}\frac{\partial g_1}{\partial \boldsymbol{F}}, \quad a_{12} = \frac{\partial f_1}{\partial \boldsymbol{F}}^T \boldsymbol{D}\frac{\partial g_2}{\partial \boldsymbol{F}} \tag{A5}$$

and re-organizing (A5) gives:

$$(A_1 + a_{11})\cdot d\lambda_1 = \frac{\partial f_1}{\partial \boldsymbol{F}}^T \boldsymbol{D}d\boldsymbol{u} - a_{12}d\lambda_2 \tag{A6}$$

The similar exercise can be done with the other surface. Multiplying with $\frac{\partial f_2}{\partial F}$ and combining with the consistency condition for the second surface:

$$\frac{\partial f_2}{\partial \boldsymbol{F}}^T\cdot d\boldsymbol{F} - A_2\cdot d\lambda_2 = 0 \tag{A7}$$

And by introducing $a_{21},\ a_{22}$:

$$a_{21} = \frac{\partial f_2}{\partial \boldsymbol{F}}^T \boldsymbol{D}\frac{\partial g_1}{\partial \boldsymbol{F}}, \quad a_{22} = \frac{\partial f_2}{\partial \boldsymbol{F}}^T \boldsymbol{D}\frac{\partial g_2}{\partial \boldsymbol{F}} \tag{A8}$$

$$(A_2 + a_{22})\cdot d\lambda_2 = \frac{\partial f_2}{\partial \boldsymbol{F}}^T \boldsymbol{D}d\boldsymbol{u} - a_{21}d\lambda_1 \tag{A9}$$

The two equations can then be combined and written:

$$d\lambda_1 = \frac{\frac{\partial f_1}{\partial \boldsymbol{F}}^T\cdot(A_2 + a_{22}) - a_{12}\frac{\partial f_2}{\partial \boldsymbol{F}}^T}{(A_1 + a_{11})\cdot(A_2 + a_{22}) - a_{12}\cdot a_{21}}\cdot\boldsymbol{D}d\boldsymbol{u} \tag{A10}$$

$$d\lambda_2 = \frac{\frac{\partial f_2}{\partial \boldsymbol{F}}^T\cdot(A_1 + a_{11}) - a_{21}\frac{\partial f_1}{\partial \boldsymbol{F}}^T}{(A_2 + a_{22})\cdot(A_1 + a_{11}) - a_{21}\cdot a_{12}}\cdot\boldsymbol{D}d\boldsymbol{u} \tag{A11}$$

Which also can be written on matrix form:

$$\begin{bmatrix} d\lambda_1 \\ d\lambda_2 \end{bmatrix} = \frac{1}{(A_2 + a_{22})\cdot(A_1 + a_{11})}\begin{bmatrix} (A_2 + a_{22}) & -a_{12} \\ -a_{21} & (A_1 + a_{11}) \end{bmatrix}\cdot\begin{bmatrix} \frac{\partial f_1}{\partial \boldsymbol{F}}^T\boldsymbol{D}d\boldsymbol{u} \\ \frac{\partial f_2}{\partial \boldsymbol{F}}^T\boldsymbol{D}d\boldsymbol{u} \end{bmatrix} \tag{A12}$$

Which we recognise as eigenvalue problem on the form:

$$\boldsymbol{x} = \boldsymbol{B}\boldsymbol{y} \tag{A13}$$

where

$$\boldsymbol{B} = \begin{bmatrix} a & c \\ b & d \end{bmatrix} => \boldsymbol{B}^{-1} = \frac{1}{\det(\boldsymbol{B})} \cdot \begin{bmatrix} d & -c \\ -b & a \end{bmatrix} \tag{A14}$$

This means that equation (A12) can be written:

$$\begin{bmatrix} f_1 \\ f_1 \end{bmatrix} = \begin{bmatrix} \frac{\partial f_1}{\partial \boldsymbol{F}}^T \boldsymbol{D} d\boldsymbol{u} \\ \frac{\partial f_2}{\partial \boldsymbol{F}}^T \boldsymbol{D} d\boldsymbol{u} \end{bmatrix} = \begin{bmatrix} (A_2 + a_{22}) & a_{12} \\ a_{21} & (A_1 + a_{11}) \end{bmatrix} \cdot \begin{bmatrix} d\lambda_1 \\ d\lambda_2 \end{bmatrix} \tag{A15}$$

And the system of equations can be expanded to include all surface 1 to k being translated:

$$\begin{bmatrix} f_1 \\ f_2 \\ \vdots \\ f_i \\ \vdots \\ f_k \end{bmatrix} = \begin{bmatrix} (A_2 + a_{22}) & a_{12} & \dots & a_{1,j} & \dots & a_{1k} \\ a_{21} & (A_1 + a_{11}) & \dots & a_{2,j} & \dots & a_{2k} \\ \vdots & \vdots & \ddots & \vdots & \dots & \vdots \\ a_{i,1} & a_{i,2} & \dots & a_{i,j} & \dots & a_{k,j} \\ \vdots & \vdots & \dots & \vdots & & \vdots \\ a_{k1} & a_{k2} & \dots & a_{kj} & \dots & A_k + a_{kk} \end{bmatrix} \cdot \begin{bmatrix} d\lambda_1 \\ d\lambda_2 \\ \vdots \\ d\lambda_i \\ \vdots \\ d\lambda_k \end{bmatrix} \tag{A16}$$

where

$$a_{i,j} = \frac{\partial f_i}{\partial \boldsymbol{F}}^T \boldsymbol{D} \frac{\partial g_j}{\partial \boldsymbol{F}} \; and \; A_i = \frac{\partial f_i}{\partial \boldsymbol{F}}^T \boldsymbol{D}_i^p \frac{\partial g_i}{\partial \boldsymbol{F}} \tag{A17}$$

References

[1] Aasen S, Page AM, Skjolden Skau K, Nygaard TA. Effect of foundation modelling on the fatigue lifetime of a monopile-based offshore wind turbine. Wind Energy Sci 2017;2:361–76. http://dx.doi.org/10.5194/wes-2-361-2017.

[2] Schafhirt S, Page A, Eiksund GR, Muskulus M. Influence of soil parameters on the fatigue lifetime of offshore wind turbines with monopile support structure. Energy Procedia 2016;94:347–56. http://dx.doi.org/10.1016/j.egypro.2016.09.194.

[3] Damgaard M, Zania V, Andersen LV, Ibsen LB. Effects of soil–structure interaction on real time dynamic response of offshore wind turbines on monopiles. Eng Struct 2014;75:388–401. http://dx.doi.org/10.1016/j.engstruct.2014.06.006.

[4] Damgaard M, Andersen LV, Ibsen LB, Toft HS, Sørensen JD. A probabilistic analysis of the dynamic response of monopile foundations: soil variability and its consequences. Probabilist Eng Mech 2015;41:46–59. http://dx.doi.org/10.1016/j.probengmech.2015.05.001.

[5] Kallehave D, Byrne BW, LeBlanc Thilsted C, Mikkelsen KK. Optimization of monopiles for offshore wind turbines. Philos Trans R Soc London A Math Phys Eng Sci 2015;373.

[6] Hald T, Mørch C, Jensen L, Bakmar KA. Revisiting monopile design using py curves. Results from full scale measurements on Horns Rev. Proc. Eur. Offshore wind 2009 conf. 2009.

[7] Tjelta T. Geotechnical experience from the installation of the Europipe jacket with bucket foundations. The offshore technology conference 1995. http://dx.doi.org/10.4043/7795-MS.

[8] Tjelta TI. Suction piles: their position and application today. Elev int offshore polar eng conf, vol. II. 2001.

[9] Bo Ibsen L, Houlsby G, Byrne B. Suction caissons for wind turbines. Front. Offshore Geotech. Taylor & Francis; 2005. http://dx.doi.org/10.1201/NOE0415390637.ch4.

[10] Senders M. Suction caissons in sand as tripod foundations for offshore wind. University of Western Australia; 2008.

[11] Byrne BW. Investigations of suction caissons in dense sand. 2000.

[12] Villalobos FA, Byrne BW, Houlsby GT, Martin CM. Bearing capacity tests of scale suction caisson footings on sand, experimental data, data report FOT005/1. 2003.

[13] Cassidy MJ, Byrne BW, Randolph MF. A comparison of the combined load behaviour of spudcan and caisson foundations on soft normally consolidated clay. Geotechnique 2004;54:91–106.

[14] Andersen K, Jostad H. Foundation design of skirted foundations and anchors in clay. The offshore technology conference 1999. http://dx.doi.org/10.4043/10824-MS.

[15] Shonberg A, Harte M, Aghakouchak A, Pachecco M, Cameron SD, Lingaard M. Suction bucket jackets for offshore wind turbines: applications from in situ observations. Proc. 19th int. Conferance soil mech. Geotech. Eng., Soul. 2017.

[16] Roscoe KH, Schofield AN. The stability of short pier foundations on sand, Discussion. Br Weld J 1957(January):12–8.

[17] Ibsen L, Barari A, Larsen K. Adaptive plasticity model for bucket foundations. J Eng Mech 2014;140:361–73. http://dx.doi.org/10.1061/(ASCE)EM.1943-7889.0000633.

[18] Villalobos Jara FA. Model testing of foundations for offshore wind turbines PhD Thesis University of Oxford; 2006

[19] Nguyen-Sy L. The theoretical modelling of circular shallow foundation for offshore wind turbines. University of Oxford; 2007.

[20] Achmus M, Akdag CT, Thieken K. Load-bearing behavior of suction bucket foundations in sand. Appl Ocean Res 2013;43:157–65. http://dx.doi.org/10.1016/j.apor.2013.09.001.

[21] Nguyen-Sy L, Houlsby GT. The theoretical modelling of a suction caisson foundation using hyperplasticity theory. Int. Symp. Front. Offshore geotech. 19-21 Sept. Perth, Australia: Taylor and Francis; 2005. p. 417–23.

[22] Cremer C, Pecker A, Davenne L. Cyclic macro-element for soil-structure interaction: material and geometrical non-linearities. Int J Numer Anal Meth GeoMech 2001;25:1257–84. http://dx.doi.org/10.1002/nag.175.

[23] Salciarini D, Tamagnini C. A hypoplastic macroelement model for shallow foundations under monotonic and cyclic loads. Acta Geotech 2009;4:163–76. http://dx.doi.org/10.1007/s11440-009-0087-2.

[24] Kafle B, Wuttke F. Cyclic Macro-element for shallow footing over unsaturated sand. 1st Pan-American conf. Unsaturated soils, PANAMUNSAT 2013. p. 521–6. http://dx.doi.org/10.13140/RG.2.1.2804.4883/2.

[25] Foglia A, Gottardi G, Govoni L, Ibsen LB. Modelling the drained response of bucket foundations for offshore wind turbines under general monotonic and cyclic loading. Appl Ocean Res 2015;52:80–91. http://dx.doi.org/10.1016/j.apor.2015.04.005.

[26] Skau KS, Chen Y, Jostad HP. A numerical study of capacity and stiffness of circular skirted foundations in clay subjected to combined static and cyclic general loading. Geotechnique 2017. http://dx.doi.org/10.1680/jgeot.16.P.092. Published:1–16.

[27] Cassidy MJ. Non-linear analysis of jack-up structures subjected to random waves. 1999.
[28] PLAXIS. PLAXIS. 2015www.plaxis.com.
[29] Grimstad G, Andresen L, Jostad HP. NGI-ADP: anisotropic shear strength model for clay. Int J Numer Anal Meth GeoMech 2012;36:483–97. http://dx.doi.org/10.1002/nag.1016.
[30] Andresen L, Petter Jostad H, Andersen K. Finite element analyses applied in design of foundations and anchors for offshore structures. Int J GeoMech 2011;11:417–30. http://dx.doi.org/10.1061/(ASCE)GM.1943-5622.0000020.
[31] Jamiolkowski M, Ladd CC, Germaine JT, Lancelotta R. New developments in field and laboratory testing of soils. Proceedings of the eleventh international conference on soil mechanics and foundation engineering. Proc. Elev. Int. Conf. Soil Mech. Found. Eng. San Francisco, USA: Balkema; 1985. p. 57–153.
[32] Andersen KH. Cyclic soil parameters for offshore foundation design. Front. Offshore geotech. III Oslo: CRC Press; 2015. http://dx.doi.org/10.1201/b18442-4 p. Chapter 2, 5–82.
[33] Skau KS, Jostad HP. Application of the NGI-procedure for design of bucket foundations for offshore wind turbines. Vol. 1, Busan, Korea. Proceedings of the twenty-fourth (2014) international ocean and polar engineering conference. 2014. p. 189–98.
[34] Prager W. The theory of plasticity: a survey of recent achievements. Arch Proc Inst Mech Eng 1847-1982 1955;1-196(169):41–57. http://dx.doi.org/10.1243/PIME_PROC_1955_169_015_02.
[35] Ziegler H. A modification to Prager's hardening rule. Q Appl Math 1959;17:55–65.
[36] Iwan WD. On a class of models for the yielding behavior of continuous and composite systems. J Appl Mech 1967;34:612–7. http://dx.doi.org/10.1115/1.3607751.
[37] Mróz Z, Norris VA, Zienkiewicz OC. An anisotropic hardening model for soils and its application to cyclic loading. Int J Numer Anal Meth GeoMech 1978;2:203–21. http://dx.doi.org/10.1002/nag.1610020303.
[38] Prévost J-H. Mathematical modelling of monotonic and cyclic undrained clay behaviour. Int J Numer Anal Meth GeoMech 1977;1:195–216. http://dx.doi.org/10.1002/nag.1610010206.
[39] Montáns FJ. Implicit multilayerJ2-plasticity using Prager's translation rule. Int J Numer Meth Eng 2001;50:347–75. http://dx.doi.org/10.1002/1097-0207(20010120)50:2<347::AID-NME28>3.0.CO;2-Q.
[40] Wichtmann T, Niemunis A, Triantafyllidis T. Strain accumulation in sand due to cyclic loading: drained triaxial tests. Soil Dynam Earthq Eng 2005;25:967–79. http://dx.doi.org/10.1016/j.soildyn.2005.02.022.
[41] Achmus M. Load bearing behaviour of bucket foundations in sand. Proceeding 3rd int symp comput geomech (ComGeoIII), Krakow, pol. 2013.
[42] Jostad HP, Grimstad G, Andersen KH, Saue M, Shin Y, You D. A FE procedure for foundation design of offshore structures – applied to study a potential OWT monopile foundation in the Korean western Sea. Geotech Eng 2014;45:63–72.
[43] Andersen KH, Berre T. Behavior of dense sand under monotonic and cyclic loading. 1999;2:667–76.
[44] Cassidy MJ, Randolph MF, Byrne BW. A plasticity model describing caisson behaviour in clay. Appl Ocean Res 2006;28:345–58. http://dx.doi.org/10.1016/j.apor.2006.08.005.
[45] Byrne BW, Cassidy MJ. Investigating the response of offshore foundations in soft clay soils. ASME 2002:263–75. http://dx.doi.org/10.1115/OMAE2002-28057.
[46] Bienen B, Byrne BW, Houlsby GT, Cassidy MJ. Investigating six-degree-of-freedom loading of shallow foundations on sand. Geotechnique 2006;56:367–79. http://dx.doi.org/10.1680/geot.2006.56.6.367.
[47] Mróz Z. On the description of anisotropic workhardening. J Mech Phys Solid 1967;15:163–75. http://dx.doi.org/10.1016/0022-5096(67)90030-0.
[48] Dafalias YF, Herman LR, Anandarajah A. Cyclic loading response of cohesive soils using a bounding surface plasticity model. Int. Conf. Recent adv. Geotech. Earthq. Eng. Soil dyn. 1981. p. 139–44. St. Louis, Missouri, USA.
[49] Puzrin AM, Houlsby GT. On the non-intersection dilemma in multiple surface plasticity. Geotechnique 2001;51:369–72. http://dx.doi.org/10.1680/geot.2001.51.4.369.
[50] Montáns FJ, Caminero MA. On the consistency of nested surfaces models and their kinematic hardening rules. Int J Solid Struct 2007;44:5027–42. http://dx.doi.org/10.1016/j.ijsolstr.2006.12.016.
[51] Koiter WT. Stress-strain relations, uniqueness and variational theorems for elastic-plastic materials with a singular yield surface. Q Appl Math 1953;11:350–4. http://dx.doi.org/10.1090/qam/59769.
[52] Grimstad G, Rønningen JA, Nøst HA. USe of IWAN models for modelling anisotropic and cyclic behaviour of clays. Numer Meth Geotech Eng 2014;I:49–55.
[53] Nygaard TA, De Vaal J, Pierella F, Oggiano L, Stenbro R. Development, verification and validation of 3DFloat; aero-servo-hydro-elastic computations of offshore structures. Energy Procedia 2016;94:425–33. http://dx.doi.org/10.1016/j.egypro.2016.09.210.
[54] Darendeli M. Development of a new family of normalized modulus reduction and material damping curves PhD. Dissertation Austin, USA: University of Texas; 2001.
[55] Carswell W, Johansson J, Løvholt F, Arwade S, Madshus C, DeGroot D, et al. Foundation damping and the dynamics of offshore wind turbine monopiles. Renew Energy 2015;80:724–36.
[56] Houlsby GT, Kelly RB, Huxtable J, Byrne BW. Field trials of suction caissons in clay for offshore wind turbine foundations. Geotechnique 2005;55:287–96. http://dx.doi.org/10.1680/geot.2005.55.4.287.
[57] Collection of papers characterizing the soil conditions at the Bothkennar site. Geotechnique 1992;42.
[58] Hight DW, Bond AJ, Legge JD. Characterization of the Bothkennaar clay: an overview. Geotechnique 1992;42:303–47. http://dx.doi.org/10.1680/geot.1992.42.2.303.
[59] Andersen KH. Bearing capacity under cyclic loading — offshore, along the coast, and on land. Can Geotech J 2009;46:513–35. http://dx.doi.org/10.1139/T09-003.